GA–A27925

HIGH INTERNAL INDUCTANCE FOR STEADY-STATE OPERATION IN ITER AND A REACTOR

by
J.R. FERRON, C.T. HOLCOMB, T.C. LUCE, J.M. PARK, E. KOLEMEN, R.J. LA HAYE, W.M. SOLOMON, and F. TURCO

SEPTEMBER 2014

GENERAL ATOMICS

DISCLAIMER

GA–A27925

HIGH INTERNAL INDUCTANCE FOR STEADY-STATE OPERATION IN ITER AND A REACTOR

by

J.R. FERRON, C.T. HOLCOMB,* T.C. LUCE, J.M. PARK,† E. KOLEMEN,‡ R.J. LA HAYE, W.M. SOLOMON,‡ and F. TURCO¶

This is a preprint of a paper to be presented at the Twenty-Fifth IAEA Fusion Energy Conf., October 13-18, 2014 in Saint Petersburg, Russia, and to be published in the *Proceedings*.

*Lawrence Livermore National Laboratory, Livermore, California.
†Oak Ridge National Laboratory, Oak Ridge, Tennessee.
‡Princeton Plasma Physics Laboratory, Princeton, New Jersey.
¶Columbia University, New York, New York.

Work supported by
the U.S. Department of Energy
under DE-FC02-04ER54698, DE-AC05-00OR22725,
DE-AC02-09CH11466, and DE-FG02-04ER54761

GENERAL ATOMICS PROJECT 30200
SEPTEMBER 2014

GENERAL ATOMICS

High Internal Inductance for Steady-State Operation in ITER and a Reactor

J.R. Ferron 1), C.T. Holcomb 2), T.C. Luce 1), J.M. Park 3), E. Kolemen 4), R.J. La Haye 1), W.M. Solomon 4), and F. Turco 5)

1) General Atomics, PO Box 85608, San Diego, CA 92186-5608, USA.
2) Lawrence Livermore National Laboratory, Livermore, CA 94550, USA.
3) Oak Ridge National Laboratory, Oak Ridge, TN 37831, USA
4) Princeton Plasma Physics Laboratory, Princeton, NJ 08543, USA
5) Columbia University, 2960 Broadway, New York, NY 10027-6900, USA.

e-mail contact of main author: ferron@fusion.gat.com

Abstract. Increased confinement and ideal stability limits at relatively high values of the internal inductance (ℓ_i) have enabled an attractive scenario for steady-state tokamak operation to be demonstrated in DIII-D. Normalized plasma pressure in the range appropriate for a reactor has been achieved in high elongation and triangularity double-null divertor discharges with $\beta_{\rm N} > 4.5$ at $\ell_i \approx 1.3$, near the ideal $n = 1$ kink stability limit calculated without the effect of a stabilizing vacuum vessel wall, with the ideal-wall limit still higher at $\beta_{\rm N} > 5.5$. Confinement is above the H-mode level with $H_{98} \approx 1.8$. At $q_{95} = 7.5$, the current is overdriven, with bootstrap current fraction $f_{\rm BS} \approx 0.8$, noninductive current fraction $f_{\rm NI} > 1$ and negative surface voltage. For ITER, operation at $\ell_i \approx 1$ is a promising option with $f_{\rm BS} \approx 0.5$ with the remainder from external current driven efficiently near the axis. This scenario has been tested in the ITER shape in DIII-D at $q_{95} = 4.8$, so far reaching $f_{\rm NI} = 0.7$ and $f_{\rm BS} = 0.4$ at $\beta_{\rm N} \approx 3.5$ with performance appropriate for the ITER Q=5 mission, $H_{89}\beta_{\rm N}/q_{95}^2 \approx 0.3$. Modeling studies explored how increased current drive power for DIII-D could be applied to maintain a stationary, fully noninductive high ℓ_i discharge. Stable solutions are found without a conducting wall at $\beta_{\rm N} = 4$, $\ell_i = 1.07$, and $f_{\rm BS} = 0.5$ and at $\beta_{\rm N} = 5$ with an ideal wall at the location of the vacuum vessel.

1. Introduction

A tokamak discharge with a relatively high value of the internal inductance ℓ_i = 1-1.5 has advantages that make it attractive for steady-state operation at high normalized pressure $\beta_{\rm N}$. Both confinement and stability improve as ℓ_i increases [1,2]. Plasmas with $\beta_{\rm N} \approx$ 4-5 are expected to be stable to low n ideal kink modes even without the effect of a conducting vacuum vessel wall [3–5]. A high ℓ_i discharge is thus a candidate for a reactor requiring high power density that could either operate stably at $\beta_{\rm N} \approx 4$ without the requirement for a nearby conducting wall or $n \geq 1$ active stabilization coils, or at $\beta_{\rm N} \approx 5$ with wall stabilization. The increase in the stability limit to $\beta_{\rm N}$ with ℓ_i requires a broad pressure profile [3,5] and is strongest with high plasma elongation κ and triangularity [4]. A broad pressure profile and strong discharge shaping both increase the bootstrap current density ($J_{\rm BS}$) in the outer half of the plasma. In addition, there is a peak in $J_{\rm BS}$ in the H-mode pedestal region. An increase in $J_{\rm BS}$ located off-axis reduces ℓ_i, introducing a challenge to maintaining an elevated value of ℓ_i as $f_{\rm BS}$ increases with $\beta_{\rm N}$. Taking this into account, an optimized compromise between high ℓ_i and high $f_{\rm BS}$ is proposed in Ref. [5], $\ell_i \approx 1$, $\beta_{\rm N}$ = 3.5-4.0, and $f_{\rm BS} \approx 0.5$. The remaining half of the current would be provided by external current drive that is efficient because the current is driven near the axis. Although the total amount of externally-driven current would be larger than in a low ℓ_i, high $q_{\rm min}$ steady-state scenario, the required external current drive power could be comparable. Operation at $\ell_i \approx 1$ is a possibility for the steady-state mission in ITER if a low pedestal height results from pedestal physics and/or ELM-stabilization using 3D fields. A reduction in the height of the H-mode pressure pedestal would increase ℓ_i, and the corresponding increase in core confinement could compensate for the reduced pedestal confinement.

This paper presents progress on the development in DIII-D of the attractive features of the high ℓ_i scenario for steady-state operation. In double null divertor discharges with both high elongation and triangularity, $\beta_N > 4.5$ has been achieved at $\ell_i \approx 1.3$. This high value of β_N is near the ideal $n = 1$ kink stability limit calculated without the effect of a stabilizing vacuum vessel wall, with the ideal wall limit still higher at $\beta_N > 5.5$. Confinement is well above the level predicted by H-mode scaling relations. In discharges with the scaled ITER shape, the optimized $\ell_i \approx 1$ scenario has been tested along with the effect of a reduction in the H-mode pedestal height. Modeling studies have been used to project parameters for stationary, high ℓ_i, fully noninductive operation in DIII-D

2. Discharge Formation

The high ℓ_i, high β_N discharges described have not yet been operated with a stationary current density (J) profile as sufficient externally-driven current is not yet available. Instead, an initial, low β_N, high ℓ_i equilibrium is established by starting the discharge with only inductive heating so that T_e is low and the characteristic timescale for relaxation of the J profile, $\tau_R \approx 0.2\,\text{s}$, is short. The discharge remains in these conditions long enough for the current profile to evolve to a stationary state [Fig. 1(a)]. Because the conductivity is very low in the outer half of the plasma, the current density profile is peaked in the core and ℓ_i reaches a relatively large asymptotic value. The minimum possible $q(0)$ (maximum $J(0)$) is desirable in order to maximize ℓ_i. The onset of sawtooth oscillations maintains $q(0) \approx 1$ and limits J near the axis, so that as I_p increases, the core J peak broadens, forming a somewhat rectangular-shaped profile (Fig. 2). After the asymptotic value of ℓ_i is reached, electron cyclotron current drive (ECCD) is added [Fig. 1(b)] near $\rho \approx 0.4$ to add

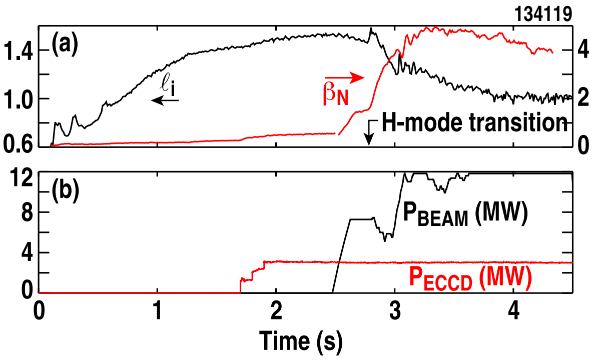

FIG. 1. Formation of the initial equilibrium with a high value of ℓ_i during the discharge shown in Fig. 3(a,b). (a) Internal inductance and β_N, (b) neutral beam and electron cyclotron heating powers.

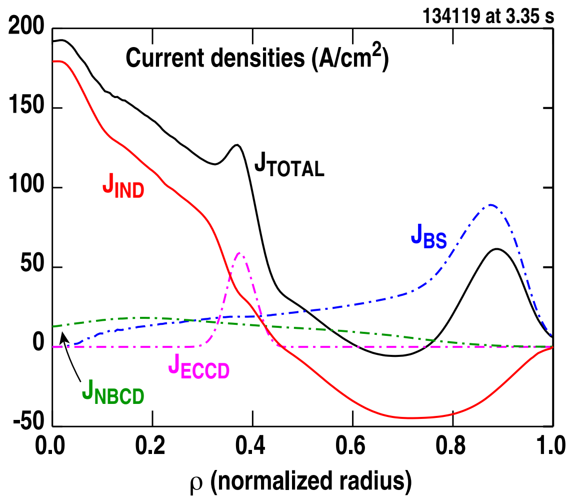

FIG. 2. Current density profiles at 3.35 s during the discharge shown in Fig. 3(a,b). The total J is obtained from an equilibrium reconstruction using experimental data, while the individual current density components were calculated using the ONETWO transport code.

externally-driven current J at the edge of the core peak (Fig. 2) and to increase T_e. The increase in T_e results in a factor of ≈ 10 increase in τ_R so that the core inductive current density ($J_{\rm IND}$) peak is essentially "frozen" in place, evolving only very slowly for the remainder of the discharge. The transition into H-mode occurs either at 2.8 s after the neutral beam heating begins (e.g. the discharge shown in Fig. 1 discussed in Secs 3 and 5) or at 1.9 s during the phase with only ECCD heating (Sec. 4). This method of forming an initial high ℓ_i equilibrium has the advantage of avoiding the rapid changes in [1,2] $I_{\rm p}$ or κ used in earlier work.

3. High Bootstrap Current Fraction, High $\beta_{\rm N}$ Discharges

In a double-null divertor configuration, discharges have been produced with $\beta_{\rm N}$ in the range required for a high power density reactor. An example is the discharge shown in Fig. 3(a,b) where $\beta_{\rm N} \approx 4.8$ for 0.4 s, dropping slowly as ℓ_i decreases from an initial value of ≈ 1.6 to about 1.0. $\beta_{\rm N} > 4$ is maintained for 1 s ($\approx 0.5\tau_R$), with excellent confinement, $H_{98} \approx 1.8$ and $H_{89} \approx 2.6$. The decrease in $\beta_{\rm N}$ with time occurs because of the decrease in confinement with ℓ_i with constant neutral beam and ECCD powers [Fig. 1(b)]. $\beta_{\rm N} > 5$ has been accessed briefly, as illustrated by the example in Fig. 3(c,d). In this case, $\beta_{\rm N}$ reaches 5 with normalized confinement above twice the prediction of scaling laws for H-mode as a result of the increased $\ell_i \approx 1.3$ during the edge-localized-mode (ELM) free phase just after the transition to H-mode. The highest $\beta_{\rm N}$ phase is terminated by the first ELM.

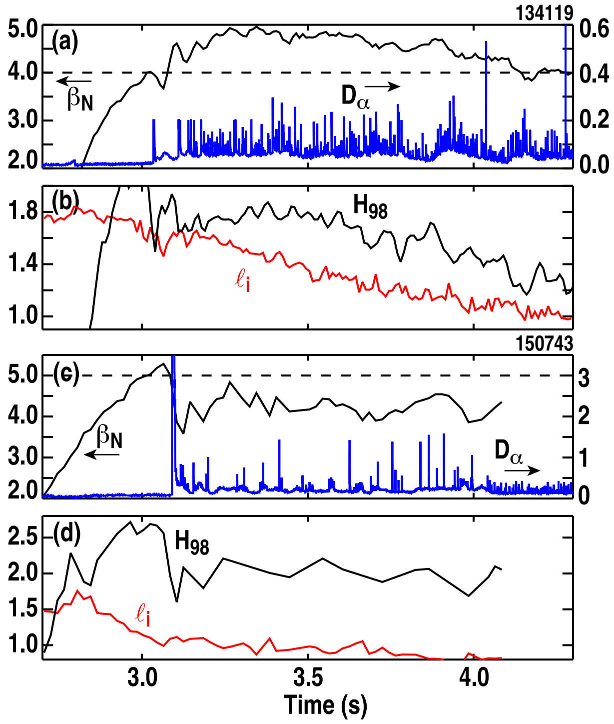

FIG. 3. Time evolution of parameters in two high ℓ_i discharges with high $\beta_{\rm N}$. A discharge with $\beta_{\rm N}$ sustained above 4: (a) $\beta_{\rm N}$ and divertor-region D_α, (b) ℓ_i and H_{98}. A discharge that has $\beta_{\rm N}$ exceeding 5 for a short interval: (c) $\beta_{\rm N}$ and divertor-region D_α, (d) ℓ_i and H_{98}. D_α units are 10^{16} photons/cm^2/s/sterrad.

These discharges have a large fraction of the current driven noninductively as a result of the high $\beta_{\rm N}$ and the relatively large $q_{95} \approx 7.5$. The total calculated noninductively driven current in the Fig. 3(a,b) discharge [Fig. 4(b)] exceeds the total plasma current as regulated using the ohmic heating coil. This is primarily because of the high $f_{\rm BS} \approx 0.8$ with the neutral-beam-driven current fraction $f_{\rm NBCD} \approx 0.2$ and the ECCD current fraction $f_{\rm ECCD} \approx 0.1$. The result is a negative surface voltage, with similar values from the measurement and the transport code calculation [Fig. 4(a)]. The surface voltage from the code is slightly more negative than from the experiment, indicating that the model somewhat over predicts the total noninductive and/or core-trapped inductive current. The current overdrive was confirmed through an increase in the total plasma current when the inductive coil current was held constant. An example is shown in Fig. 5 where, for the discharge shown in red, the inductive coil current was held fixed beginning at 2.6 s, resulting in an increase in the total current as β_N increased, a decrease in q_{95}, and access to higher β_T.

It is the evolution of the toroidal electric field profile that primarily determines the time evolution of ℓ_i. The peak in J_{BS} in the H-mode pedestal region is relatively broad (Fig. 2) as a result of the high value of $\beta_P \leq 3.4$ so it accounts for a significant amount of off-axis current. However, the J_{BS} profile and the bootstrap current fraction remain roughly constant during the high β_N phase of the discharge, with only a small shift of current density from the H-mode pedestal region to the discharge core as β_N decreases and the pressure profile becomes more peaked (Sec. 5). This change would tend to increase ℓ_i. There is a small increase with time in the modeled f_{NBCD} and f_{ECCD} as a result of decreasing electron density. The negative surface voltage, though, penetrates relatively quickly through the outer half of the discharge, so that the calculated inductive electric field is zero at $\rho = 0.5$ by the time β_N reaches its peak value (as indicated by J_{IND} in Fig. 2). The negative inductively-driven current density in the outer half of the discharge offsets some of the bootstrap current, helping to maintain the elevated value of ℓ_i. The negative electric field penetrates slowly through the discharge core, with the modeled field reaching zero at $\rho = 0.4$ by 3.8 s, but remaining positive to the end of the discharge at $\rho = 0.3$. The total inductively-driven current in the discharge core gradually decreases so that the negative surface voltage required to offset the noninductive current overdrive also decreases with time, resulting in the slow decrease in ℓ_i. The discharge

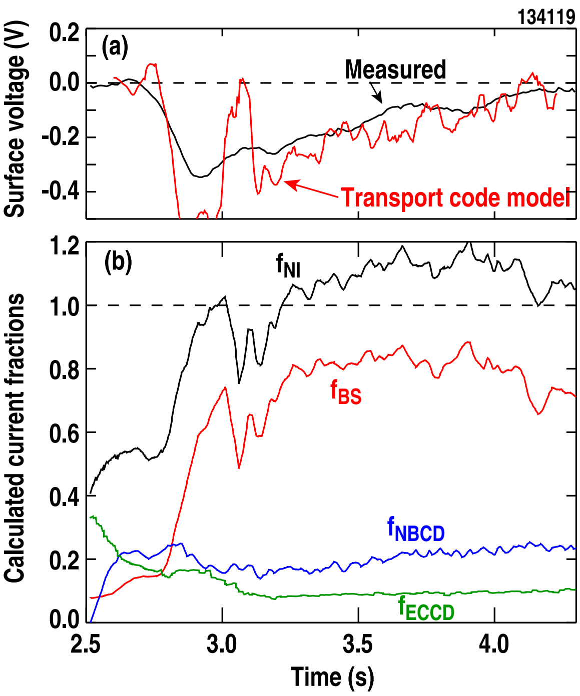

FIG. 4. Parameters for the discharge shown in Fig. 3(a,b). (a) Measured and transport-code-calculated surface voltage, (b) noninductive current fraction (f_{NI}), bootstrap current fraction (f_{BS}), fraction of neutral-beam-driven current (f_{NBCD}), and fraction of ECCD current (f_{ECCD}).

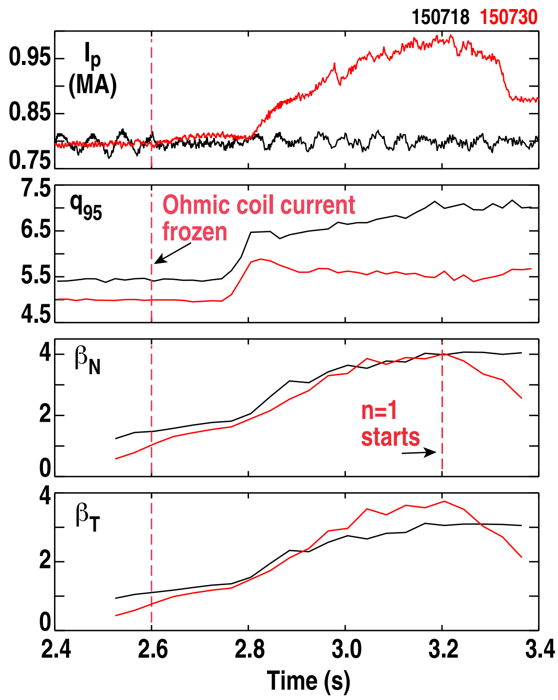

FIG. 5. Parameters in two discharges that were formed similarly except that for the discharge shown in red, the the current in the inductive heating coil was held fixed beginning at 2.6 s.

evolves toward a stationary state with a relatively low ℓ_i because of the off-axis bootstrap current. With additional current drive power, the evolving $J_{\rm IND}$ profile could be replaced with stationary profiles of $J_{\rm NBCD}$ and $J_{\rm ECCD}$ (Sec. 6).

4. Discharges in the ITER Scaled Shape

Discharge conditions compatible with an optimized $\ell_i \approx 1$ scenario [5] are a possibility for ITER. The H-mode pedestal pressure could be too low to achieve the target fusion gain for the steady-state mission in the high $q_{\rm min} \approx 2$, relatively low $\ell_i < 0.8$ scenario often discussed [6]. ELM mitigation using 3D magnetic fields, for instance, can reduce the pedestal density and pressure. A reduction in the pedestal pressure reduces $J_{\rm BS}$ near the plasma boundary, leading naturally to increased ℓ_i. The types of current drive sources planned for ITER, neutral beam and ECCD, could provide the core current density required to maintain $q_{\rm min} \approx 1$ to maximize ℓ_i.

Discharges with the planned ITER shape, scaled to fit into the DIII-D vacuum vessel, were produced with the goal of testing the optimized $\ell_i \approx 1$, $f_{\rm BS} \approx 0.5$ scenario. With $q_{95} = 4.8$, near the value envisioned for steady-state operation in ITER [6], the experiment has thus far operated with $f_{\rm NI} \approx 0.7$, $f_{\rm BS} \approx 0.4$ and $\beta_{\rm N} \approx 3.5$ [Fig. 6(b,d)]. The initial $\ell_i \approx 1.25$ is lower than in the Fig. 3 discharges [Fig. 6(a)] as a result of the reduction in q_{95}. However, ℓ_i is still ≈ 1 at the end of the discharge because of reduced total bootstrap current in the H-mode pedestal region. The reduced pedestal bootstrap current results from the change to the single-null divertor shape, lower $\beta_{\rm P}$, and lower $\beta_{\rm N}$, so that the H-mode pedestal pressure is reduced and the $J_{\rm BS}$ peak is narrower. Discharge performance is close to the estimated requirement for the ITER steady-state mission with $G = \beta_{\rm N} H_{89}/q_{95}^2 \approx 0.3$ [Fig. 6(c)].

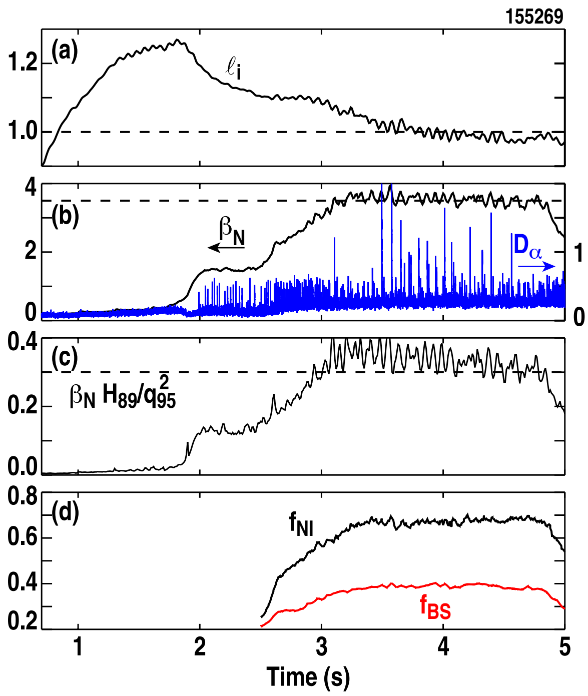

FIG. 6. Parameters in a discharge operated in the ITER scaled shape. (a) internal inductance, (b) $\beta_{\rm N}$ and divertor-region D_α, (c) the fusion gain factor G, (d) noninductive and bootstrap current fractions. D_α units are 10^{15} photons/cm^2/s/sterrad.

The effect of a reduction in the H-mode pedestal pressure on the current density profile was tested by applying $n = 3$ fields from the DIII-D I coils [7] (Fig. 7). The four discharges in the figure were initiated identically and had similar parameters before the I coil current was turned on at 2.1 s. With the I coil current, the pedestal pressure decreased as the strength of the $n = 3$ field was increased. As anticipated, the corresponding modifications to the current density profile resulted in evolution to a higher value of ℓ_i in the discharges with the lower pedestal pressure.

5. Stability Limits to β_N

Global, ideal MHD, low toroidal mode number (n) pressure and current driven instabilities, which are expected to set the ultimate limit to pressure in these discharges, have not yet been clearly observed. In the cases where stability determines the limit to performance, the observed mode is most commonly an $m = 2/n = 1$ resistive tearing mode that often follows immediately after a fishbone-like or internal kink-like 1/1 burst detected on the Mirnov probes. At $q_{95} \approx 7$, the 2/1 mode can limit duration with the maximum β_N limited by confinement. At $q_{95} = 4.5$ to 6, the 2/1 mode has limited β_N to 3.8-4. In both cases, there has been some success in avoiding the 2/1 mode with ECCD deposited at or near the $q = 2$ surface.

The high values of β_N attained at high ℓ_i are consistent with the calculated ideal MHD $n = 1$ stability limits (Fig. 8). The double-null discharge (Sec. 3) had β_N very close to the no-wall limit [Fig. 8(a)], while the attainable β_N in the ITER-shape discharge was limited by the 2/1 resistive mode to a value below both ideal stability limits [Fig. 8(b)]. The stability limits were calculated using the DCON code to evaluate equilibria with plasma pressure profiles scaled by a uniform factor at constant q profile from the original equilibrium reconstructed from the experimental data. There is uncertainty in the calculation result, as indicated by the scatter in the data points in the figure, that arises from the sensitivity to the details of the equilibrium and the stability limit calculation method.

The stability limits to β_N can be high in these discharges because of the increased values of ℓ_i and also because the plasma pressure profiles are relatively

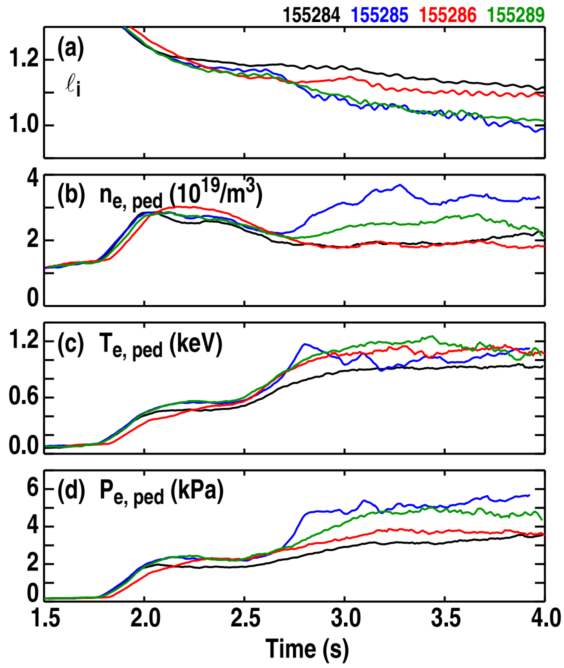

FIG. 7. Discharges at $q_{95} = 5.5$, $\beta_N = 3$ produced in the same way except for the current in the I-coils [7]. Blue curves: no I-coil current; green curves: 2 kA coil current both coil rows even parity, red curves: 5.5 kA both coil rows, even parity; black curves: 5.5 kA, lower I-coil row only. (a) Internal inductance, (b) electron density at the top of the H-mode pedestal, (c) pedestal electron temperature, (d) pedestal electron pressure.

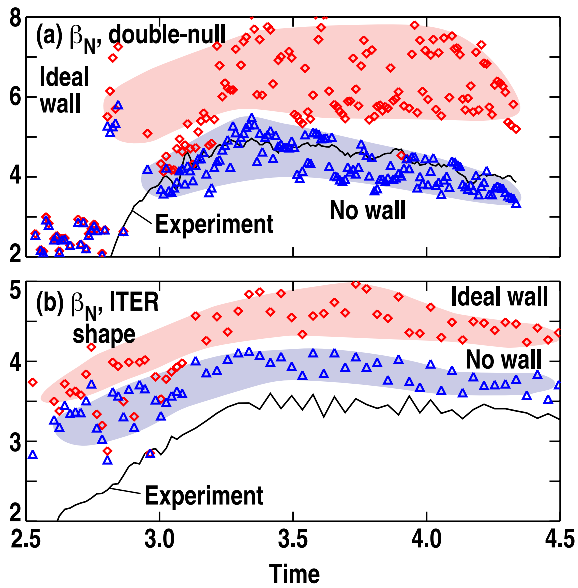

FIG. 8. Ideal MHD $n = 1$ stability limits calculated without including the effect of the conducting vacuum vessel wall (blue) and including the wall (red). (a) Double-null divertor shape discharge shown in Fig. 3(a,b), (b) ITER shape discharge shown in Fig. 6.

broad, as indicated by the low pressure peaking factor $f_\mathrm{p} = P(0)/\langle P\rangle$ (Fig. 9). The initial decrease in f_p is consistent with [8] where a broadening of the core pressure profile and a corresponding decrease in f_p is observed with an increase in β_N. The gradual increase in f_p during the high β_N phase is likely a result of decreasing β_N, but could also be a result of changes in the core magnetic shear profile shape as ℓ_i decreases. Similarly, the higher f_p in the ITER-shape case could indicate a dependence on the discharge shape, but the differences likely result from the higher β_N in the double-null. The lower calculated stability limits for the ITER-shape discharge (Fig. 8) are expected as a result of the changes in both the shape and f_p.

In the discharges with $n = 3$ fields applied (Fig. 7), the values of both ℓ_i and f_p play a role in determining the β_N stability limit. The two cases with the highest I coil current have a significantly increased f_p [Fig. 10(b)] that is reflected in a reduction in the calculated ideal-wall stability limit [Fig. 10(a)]. The no-wall stability limit, however, shows no dependence on the I coil current, possibly because the increase in f_p is offset by the increased ℓ_i in those discharges.

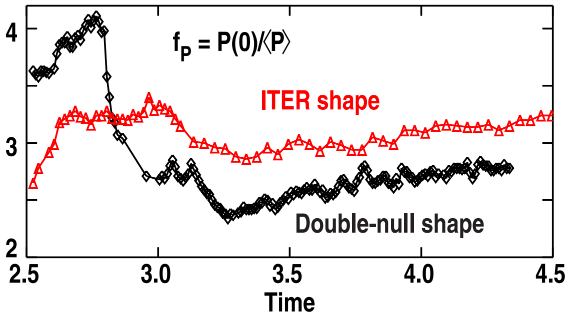

FIG. 9. Measured pressure peaking factor $f_\mathrm{p} = P(0)/\langle P\rangle$ for the double-null divertor shape discharge shown in Fig. 3(a,b) (black) and the ITER shape discharge shown in Fig. 6 (red).

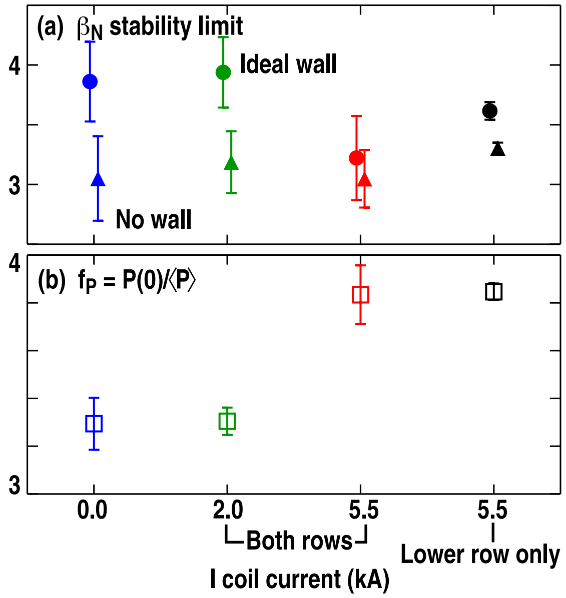

FIG. 10. Parameters averaged over the interval 3-4 s for the discharges shown in Fig. 7. (a) Ideal MHD stability limits calculated without the vacuum vessel wall (triangles) and with the vessel wall (circles). (b) Pressure peaking factor.

6. Modeling of a Stationary High ℓ_i Discharge for DIII-D

Modeling predicts that parameters for stationary, high ℓ_i, fully noninductive operation are attainable in DIII-D. Studies with model equilibria documented the scaling of ℓ_i with the H-mode pedestal current density (Fig. 11). An increase of ℓ_i from 0.75 to 1.3 requires a factor of two decrease in the pedestal current, with $\ell_i \approx 1$ at about 75% of the reference experimental value. There is a corresponding increase in the $n = 1$ no-wall β_N limit, which reaches $\beta_\mathrm{N} \approx 5$ with $\ell_i \approx 1.3$, similar to what was observed in the double-null experimental discharges. Thus there is a significant advantage in stability if current density is shifted from the pedestal region to the core. In order to maintain $q(0) > 1$ to avoid sawteeth, the width of the current density peak at the axis must increase as q_{95} is reduced, so that some of the externally-driven current must be located off-axis. Studies with the FASTRAN transport code using the TGLF energy transport model explored how the increased current drive power in a proposed DIII-D upgrade (13 MW off-axis neutral beam, 9 MW ECCD) could be applied to maintain a stationary, $f_{\mathrm{NI}} = 1$ high ℓ_i discharge. In the solution, $\ell_i = 1.07$, $\beta_{\mathrm{N}} = 4$, $f_{\mathrm{BS}} = 0.5$, and the no-wall ideal $n = 1$ stability limit is $\beta_{\mathrm{N}} \approx 4.1$. The bootstrap current density profile is broad (Fig. 12) and off-axis neutral beam current drive coupled with ECCD close to the axis is used to generate the current density peak extending to $\rho \approx 0.4$ that maintains the increased value of ℓ_i. By injecting the neutral beams off-axis, the fast ion profile is less peaked, contributing to an increase in the stability limit. A similar solution at $\beta_{\mathrm{N}} \approx 5$ that takes advantage of wall stabilization was also found.

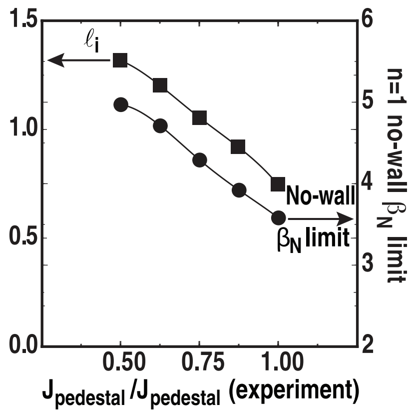

FIG. 11. Scaling in model equilibria of ℓ_i (squares) and the calculated $n = 1$ no-wall β_{N} limit (circles) with the H-mode pedestal current density.

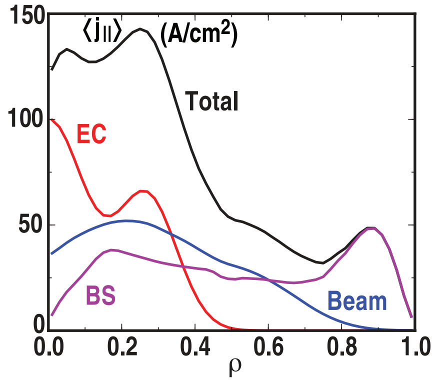

FIG. 12. Current density profiles in the $\beta_{\mathrm{N}} = 4$ transport code-modeled steady-state solution for DIII-D.

7. Conclusion

Modeling and experiment are showing the potential of a high ℓ_i discharge for fully noninductive, stationary operation. High values of $\beta_{\mathrm{N}} > 4.5$ and H_{98} have been demonstrated in the experiment and with $q_{95} \approx 7.5$, f_{BS} has reached 0.8. In order to attain the high values of toroidal β required for a reactor, q_{95} must be reduced. Keys to full development of this scenario are an understanding of how to maximize ℓ_i through access to appropriate pedestal parameters, avoidance of the performance limiting $n = 1$ tearing mode, and demonstration of the total required externally-driven current near the axis. Operation at relatively high values of ℓ_i could be a good option for ITER, depending on the value of the pedestal pressure.

This material is based upon work supported by the U.S. Department of Energy, Office of Science, Office of Fusion Energy Sciences, using the DIII-D National Fusion Facility, a DOE Office of Science user facility, under Awards DE-FC02-04ER54698, DE-AC52-07NA27344, DE-AC05-00OR22725, DE-AC02-09CH11466, and DE-FG02-0454761.

References

[1] FERRON, J.R., *et al.,* Phys. Fluids B **5**, 2532 (1993).
[2] LAO, L.L., *et al.,* Phys. Plasmas **5**, 1050 (1998).
[3] HOWL, W., *et al.,* Phys. Fluids B **4**, 1731 (1992).
[4] TURNBULL, A.D., *et al.,* Nucl. Fusion **38**, 1467 (1998).
[5] LIN-LIU, Y.R., *et al.,* Phys. Plasmas **6**, 3934 (1999).
[6] POLI, F.M., *et al.,* Nucl. Fusion **54**, 073007 (2014).
[7] EVANS, T.E., *et al.,* Phys. Plasmas **13**, 056121 (2006).
[8] FERRON, J.R., *et al.,* Nucl. Fusion **51**, 063026 (2011).